drones

MDPI

Article

Using Semicircular Sampling to Increase Sea-Wind Retrieval Altitude with a High-Altitude UAV Scatterometer

Alexey Nekrasov [1,2,*], Alena Khachaturian [1] and Colin Fidge [3]

[1] Department of Radio Engineering Systems, Saint Petersburg Electrotechnical University, Professora Popova 5F, 197022 Saint Petersburg, Russia
[2] Institute for Computer Technologies and Information Security, Southern Federal University, Chekhova 2, 347922 Taganrog, Russia
[3] Faculty of Science, Queensland University of Technology (QUT), Gardens Point Campus, Brisbane, QLD 4001, Australia
* Correspondence: alexei-nekrassov@mail.ru; Tel.: +7-8634-360-484

Abstract: Currently, unmanned aerial vehicles (UAVs) are widely used due to their low cost and flexibility. In particular, they are used in remote sensing as airborne platforms for various instruments. Here, we investigate the capability of a conical scanning radar operated as a scatterometer mounted on a high-altitude UAV to perform sea surface wind retrieval based on an appropriate geophysical model function (GMF). Increasing the maximum altitude of the wind retrieval method's applicability is an important problem for UAV or manned aircraft scatterometers. For this purpose, we consider the possibility of increasing the method's maximum altitude by applying a semicircular scheme for azimuth normalized radar cross section (NRCS) sampling instead of a whole 360° circular scheme. We developed wind retrieval algorithms for both semicircular and circular NRCS sampling schemes and evaluated them using Monte Carlo simulations. The simulations showed that the semicircular scheme for azimuth NRCS sampling enables twice the maximum altitude for wind retrieval compared to a 360° circular scheme. At the same time, however, the semicircular scheme requires approximately three times the number of integrated NRCS samples in each azimuth sector to provide equivalent wind retrieval accuracy. Nonetheless, our results confirm that the semicircular azimuth NRCS sampling scheme is well-suited for wind retrieval, and any wind retrieval errors are within the typical range for scatterometer wind recovery. The obtained results can be used for enhancing existing UAV and aircraft radars, and for the development of new remote sensing systems.

Keywords: UAV; conical scanning radar; airborne scatterometer; radar backscatter; sea surface; sea-wind retrieval

check for updates

Citation: Nekrasov, A.; Khachaturian, A.; Fidge, C. Using Semicircular Sampling to Increase Sea-Wind Retrieval Altitude with a High-Altitude UAV Scatterometer. *Drones* **2022**, *6*, 223. https://doi.org/10.3390/drones6090223

Academic Editors: Miroslaw Zimnoch and Paweł Ćwiąkała

Received: 20 July 2022
Accepted: 24 August 2022
Published: 26 August 2022

1. Introduction

An unmanned aerial vehicle (UAV), also called a drone, is an aircraft that has no pilot, crew, or passengers on board. A UAV is a unit of an unmanned aircraft system (UAS) [1]. UASs include air vehicles and associated equipment (e.g., ground-based controllers and communication systems). UASs do not carry a human operator, and they can operate autonomously or be piloted remotely [2].

Advances in miniaturization of equipment and data processing systems have led to the rapid development and production of UAVs as airborne platforms for various remote sensing instruments [3]. In recent decades, they have become widely used tools due to their relatively low cost and flexibility [4,5].

Currently, UAVs have a wide range of applications [3]. For instance, they are used in power line, pipeline, ship, mine, and dam inspection; anomaly detection and intrusion prevention; forest monitoring and protection, early fire detection and extinguishing; hazard, traffic, and environmental monitoring; search and rescue operations; emergency response; border and harbor patrol; police surveillance; aerial photography; SWAT support;

mapping and imaging; intelligence, surveillance, and reconnaissance; chemical spraying; crop dusting; night vision; and entertainment industry and filming [6–10]. Typically, UAVs are categorized based on their weight, speed, altitude, range, endurance, as well as payload [3,11–13].

Depending on their application, UAVs can be equipped with appropriate sensors for obtaining information on an object of interest remotely. Thus, UAV sensors play a significant role in local remote sensing, to improve and supplement the results of global remote sensing, and remote sensing applications of UAVs are ever-expanding due to significant research and commercial interest in their use [11].

Some of the many promising UAV applications also relate to measuring the atmosphere, ocean, and air–sea interactions. Depending on UAV characteristics, some UAVs are also able to fly at a high altitude of up to 30,000 m [14].

A well-known example of a remote sensing instrument developed for high-altitude UAVs is the High-Altitude Imaging Wind and Rain Airborne Profiler (HIWRAP). HIWRAP is a dual-frequency (Ku- and Ka-bands) dual-beam (30° and 40° incidence angles) conical scanning airborne Doppler radar designed to operate on NASA's Global Hawk UAV at an altitude of about 20 km [15–17]. The radar has been designed especially to: measure atmospheric winds using precipitation and clouds as tracers; measure ocean surface winds using wind scatterometry; map 3-dimensional winds and precipitation within hurricanes and other severe weather events; and map ocean surface winds in clear to light rain regions using scatterometry.

Analysis of the HIWRAP measuring geometry shows that its 40° incidence angle beam traces a water-surface circle with a diameter of 33.56 km from a 20 km altitude. A relatively smaller traced circle diameter of 23.09 km is provided by the 30° incidence angle beam at the same altitude.

Recently, we have considered sea-wind retrieval by various airborne instruments operated in a scatterometer mode: an FM-CW millimeter wave demonstrator system [18], an airborne Doppler navigation system [19,20], an airborne weather radar [21,22], and an airborne scatterometer with a rotating antenna [23,24] at the circular ground track. Circular normalized radar cross section (NRCS) measurements performed at the single incidence angle were used for this purpose. The whole circular NRCS curve was within the area observed, and its dimensions did not exceed 15–20 km diameter. As the area under observation does not exceed these relatively small dimensions, it can usually be safely assumed that the area has the same wind and wave conditions in all of its parts. Additionally, the dimensions of the observed area (the diameter of the circular NRCS curve) limit the wind retrieval method's applicable maximum altitude based on the whole 360° circular NRCS curve [23,25].

Consequently, for the HIWRAP or a similar conical scanning radar configuration, the maximum altitudes of applicability of the wind retrieval method using the whole 360° circular NRCS curve are 17.32 km and 11.92 km at the incidence angles of 30° and 40°, respectively. From the abovementioned HIWRAP operating altitude and related diameters of the water-surface circles observed, we can see that they can exceed their physical limitations, allowing the wind and wave conditions to be effectively identical in all parts of the area observed. So, the whole 360° circular NRCS curve is not used for wind retrieval with the HIWRAP at the operating altitude of 20 km, and the wind retrieval procedure is based on NRCSs corresponding only to several different azimuth angles relative to its ground track.

In this connection, increasing the maximum altitude of the wind retrieval method's applicability is an important problem for UAV or manned aircraft scatterometers or multifunctional radars with the scatterometer mode. Therefore, our research investigated the possibility of increasing the maximum altitude of the method's applicability by using only half of the circular NRCS curve for wind retrieval by a scatterometer mounted on a high-altitude remote sensing UAV or aircraft.

2. Materials and Methods

Let a UAV equipped with a conical scanning scatterometer (e.g., HIWRAP or similar conical scanning radar operated in the scatterometer mode) make a horizontal straight flight at speed V and altitude H over the sea. Let the conical scanning geometry of the scatterometer be as presented in Figure 1.

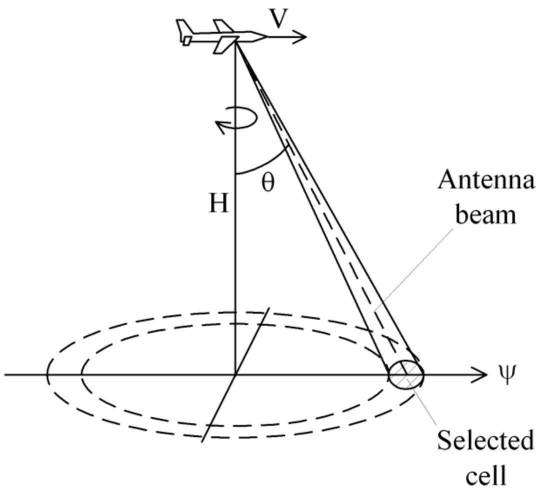

Figure 1. Geometry of the conical scanning scatterometer: V is the speed of flight; H is the altitude; θ is the incidence angle; and ψ is the UAV's flight direction.

In the general case, when the UAV's altitude and incidence angle θ combine so that the diameter of the observed circular NRCS curve does not exceed 15–20 km, and the wind and wave conditions in all parts of the observed area are effectively identical, then the whole 360° circular NRCS curve obtained at the same incidence angle can be used for wind retrieval over the sea. In this case, the whole 360° circular NRCS curve is represented by an N azimuth sector observed with the given azimuth step, e.g., of 5° or 10°, which is equal to the width of the azimuth sector $\Delta\alpha_s$, and the wind speed and direction can be found by means of the system of N equations composed for NRCSs of the appropriate azimuth sector with the help of the geophysical model function (GMF) [24]:

$$\begin{cases} \sigma^\circ(U,\theta,\alpha+\psi_1) = A(U,\theta) + B(U,\theta)\cos(\alpha+\psi_1) + C(U,\theta)\cos(2(\alpha+\psi_1)), \\ \cdots\cdots\cdots\cdots\cdots\cdots\cdots\cdots\cdots\cdots \\ \sigma^\circ(U,\theta,\alpha+\psi_i) = A(U,\theta) + B(U,\theta)\cos(\alpha+\psi_i) + C(U,\theta)\cos(2(\alpha+\psi_i)), \\ \cdots\cdots\cdots\cdots\cdots\cdots\cdots\cdots\cdots\cdots \\ \sigma^\circ(U,\theta,\alpha+\psi_N) = A(U,\theta) + B(U,\theta)\cos(\alpha+\psi_N) + C(U,\theta)\cos(2(\alpha+\psi_N)), \end{cases} \quad (1)$$

where $i = \overrightarrow{1,N}$, $N = 360^\circ/\Delta\alpha_s$, $\sigma^\circ(U,\theta,\alpha+\psi_i)$ is the measured NRCS corresponding to azimuth sector i; U is the wind speed; α is the azimuth angle counted from the upwind direction; ψ_i is the direction of azimuth sector i relative to the aircraft course ψ; $A(U,\theta)$, $B(U,\theta)$, and $C(U,\theta)$ are the coefficients given as $A(U,\theta) = a_0(\theta)U^{\gamma_0(\theta)}$, $B(U,\theta) = a_1(\theta)U^{\gamma_1(\theta)}$, $C(U,\theta) = a_2(\theta)U^{\gamma_2(\theta)}$; and $a_0(\theta)$, $a_1(\theta)$, $a_2(\theta)$, $\gamma_0(\theta)$, $\gamma_1(\theta)$, and $\gamma_2(\theta)$ are the coefficients corresponding to the used incidence angle, radar wavelength, and transmit and receive polarization, respectively. The applicability of the GMF, used in Equation (1), which depends on the antenna beamwidth in the azimuth plane (width of the azimuth sector $\Delta\alpha_s$), was proven in our previous work [26,27].

Going back to the HIWRAP beam configuration, even considering its lowest incidence angles of 30°, wind retrieval by Equation (1) can be performed only up to 17.32 km altitude, which is lower than HIWRAP's operating altitude of 20 km. As a modern UAV's ceiling is up to 30,000 m [15], increasing the maximum altitude of the method's applicability, preferably without reducing its wind retrieval accuracy, is an important problem.

Taking into account the azimuth features of the GMF and trying to use the maximum possible number of the azimuth sectors observed in the whole 360° circular NRCS curve, we instead separate wind retrieval for two sets of sectors: the right-side sectors of the circle within the azimuths from 0° to 180°, and the left-side sectors of the circle within the azimuths from 180° to 360° relative to the UAV ground track. Thus, the ground strip with the circular NRCS curve is divided into two equal ground strips containing their own semicircles of the whole 360° circular NRCS curve observed. As the semicircular ground strip is half as wide as the circular ground strip, the maximum altitude of the method's applicability can be doubled. Therefore, the maximum altitude of the method's applicability at the incidence angle of 30° is increased to 34.64 km.

In the case of the right-side semicircle's sea-wind retrieval, the following system of equations can be used:

$$\begin{cases} \sigma^\circ(U,\theta,\alpha+\psi_1) = A(U,\theta) + B(U,\theta)\cos(\alpha+\psi_1) + C(U,\theta)\cos(2(\alpha+\psi_1)), \\ \cdots\cdots\cdots\cdots\cdots\cdots\cdots\cdots\cdots\cdots\cdots\cdots\cdots\cdots\cdots\cdots \\ \sigma^\circ(U,\theta,\alpha+\psi_i) = A(U,\theta) + B(U,\theta)\cos(\alpha+\psi_i) + C(U,\theta)\cos(2(\alpha+\psi_i)), \\ \cdots\cdots\cdots\cdots\cdots\cdots\cdots\cdots\cdots\cdots\cdots\cdots\cdots\cdots\cdots\cdots \\ \sigma^\circ(U,\theta,\alpha+\psi_{N/2+1}) = A(U,\theta) + B(U,\theta)\cos(\alpha+\psi_{N/2+1}) + C(U,\theta)\cos(2(\alpha+\psi_{N/2+1})). \end{cases} \quad (2)$$

Similarly, the wind over the sea can be retrieved from the left-side semicircle:

$$\begin{cases} \sigma^\circ(U,\theta,\alpha+\psi_{N/2+1}) = A(U,\theta) + B(U,\theta)\cos(\alpha+\psi_{N/2+1}) + C(U,\theta)\cos(2(\alpha+\psi_{N/2+1})), \\ \cdots\cdots\cdots\cdots\cdots\cdots\cdots\cdots\cdots\cdots\cdots\cdots\cdots\cdots\cdots\cdots \\ \sigma^\circ(U,\theta,\alpha+\psi_i) = A(U,\theta) + B(U,\theta)\cos(\alpha+\psi_i) + C(U,\theta)\cos(2(\alpha+\psi_i)), \\ \cdots\cdots\cdots\cdots\cdots\cdots\cdots\cdots\cdots\cdots\cdots\cdots\cdots\cdots\cdots\cdots \\ \sigma^\circ(U,\theta,\alpha+\psi_N) = A(U,\theta) + B(U,\theta)\cos(\alpha+\psi_N) + C(U,\theta)\cos(2(\alpha+\psi_N)), \\ \sigma^\circ(U,\theta,\alpha+\psi_1) = A(U,\theta) + B(U,\theta)\cos(\alpha+\psi_1) + C(U,\theta)\cos(2(\alpha+\psi_1)). \end{cases} \quad (3)$$

Finally, the wind direction ψ_w is converted from the up-wind direction [28]:

$$\psi_w = \psi - \alpha \pm 180^\circ, \quad (4)$$

where the $\pm$ sign before 180° means that 180° is adding in the case of $0^\circ \leq \psi - \alpha < 180^\circ$, and 180° is subtracting in the case of $180^\circ \leq \psi - \alpha < 360^\circ$, as an azimuth angular value in navigation should always be within the interval [0°, 360°].

Thus, splitting the whole 360° circular NRCS curve observed by the conical scanning scatterometer into two semicircles and using the retrieved wind speed and direction from each semicircle should double the maximum altitude of the method's applicability.

3. Results and Discussion

To verify the applicability of our new wind retrieval scheme and algorithm where only a semicircular NRCS curve is used to retrieve the wind vector, we performed a simulation corresponding to the HIWRAP incidence angles of 30° and 40°. We performed Monte Carlo simulations using a Ku-band GMF of the form presented by Spencer and Graf [29], with a Rayleigh Power (Exponential) distribution, fitted to Equations (1)–(3) above with the coefficients for the horizontal transmit and receive polarization from [30]:

$$\begin{aligned} a_0(\theta) &= 10^{2.47324-0.22478\theta+0.001499\theta^2} &, a_1(\theta) &= 10^{-0.50593-0.116694\theta+0.000484\theta^2}, \\ a_2(\theta) &= 10^{1.63685-0.21004888\theta+0.0013383\theta^2} &, \gamma_0(\theta) &= -0.15+0.071\theta-0.0004\theta^2, \\ \gamma_1(\theta) &= -0.02+0.061\theta-0.0003\theta^2 &, \gamma_2(\theta) &= -0.16+0.074\theta-0.0004\theta^2. \end{aligned} \quad (5)$$

Wind retrieval was evaluated in a wind speed range from 2 m/s to 30 m/s.

For the simulation, we assumed that the azimuth NRCS curves consisted of azimuth sectors of 5° width. Thus, the whole 360° circular NRCS curve consisted of N = 72 azimuth sectors with azimuths from 0° to 355°, and the right-side semicircle NRCS curve consisted of N = 37 azimuth sectors with azimuths from 0° to 180°.

First, we evaluated the wind retrieval errors arising in the case of wind retrieval with the whole 360° circular scheme. A total of 87 "measured" NRCS samples were generated for each azimuth sector, assuming a 0.2 dB instrumental noise.

Figures 2 and 3 demonstrate the simulation results of the wind retrieval errors in the case of the whole 360° circular scheme when 87 samples are integrated in the azimuth sector at incidence angles of 30° and 40°, respectively. The wind retrieval maximum errors are 0.73 m/s and 5.6° at θ = 30°, and 0.64 m/s and 4.5° at θ = 40°, respectively.

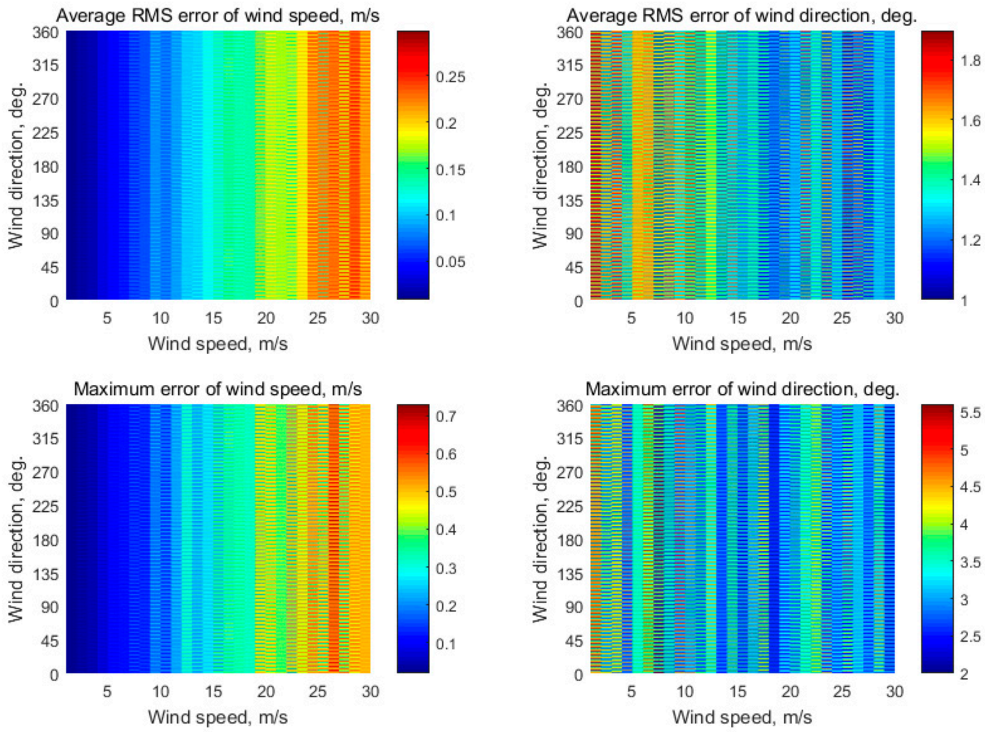

Figure 2. Simulation results in the case of the whole 360° circular scheme (observation of N = 72 azimuth sectors at the directions of 0°, 5°, 10°, . . . 355° relative to the aircraft's course) when 87 NRCS samples are integrated in each azimuth sector at an incidence angle of 30° with an assumption of 0.2 dB instrumental noise at wind speeds of 2–30 m/s.

Then, we evaluated wind retrieval with our semicircular scheme. The right-side semicircular NRCS curve consisted of N = 37 azimuth sectors with azimuths from 0° to 180°. As this scheme covers only half of the full NRCS circle, it uses half as many azimuth sectors than the whole 360° circular scheme. This would lead to increasing the wind retrieval errors and even to ambiguous measuring of the wind direction if the number of integrated NRCS samples in the azimuth sector in the semicircular scheme was the same as in the circular scheme. The wind direction ambiguity mostly arises from two opposite wind directions at similar wind speeds due to the azimuth features of the water GMF [31]. The azimuth NRCS curve at medium incidence angles is smooth and has its largest maximum in the upwind direction and the second-largest maximum in the downwind direction, while its two minima are near the crosswind direction shifted slightly to the second-largest maximum [32]. A small difference between the NRCS value at the maxima and between the largest maximum and the corresponding minima, along with considerable NRCS spread, may cause a wind direction ambiguity which, i.e., in the case of a three-beam satellite scatterometer, may appear in up to four different wind directions [31,33]. A way to decrease the statistical fluctuation of NRCS and, as a consequence, its influence on wind retrieval accuracy, is by increasing the number of integrated NRCS samples [34]. Therefore, to avoid possible ambiguity in the wind direction retrieval and to reduce wind retrieval errors in the semicircular scheme to the level of the whole 360° circular scheme, the number of integrated NRCS samples must be increased for the semicircular scheme.

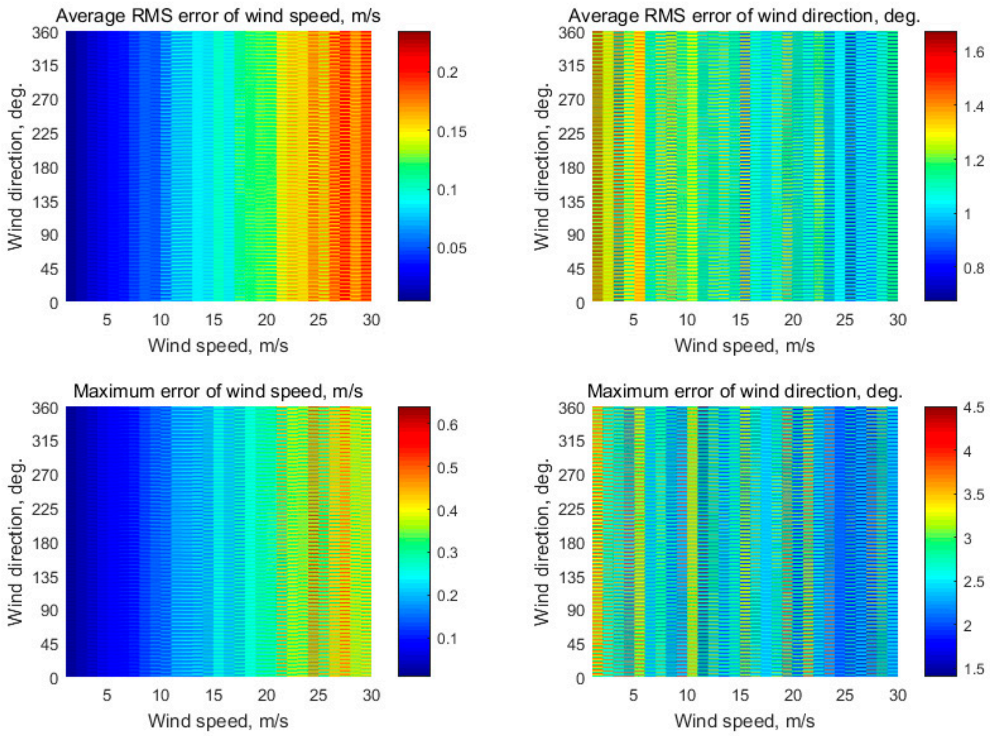

Figure 3. Simulation results in the case of the whole 360° circular scheme (observation of N = 72 azimuth sectors at the directions of 0°, 5°, 10°, . . . 355° relative to the aircraft's course) when 87 NRCS samples are integrated in each azimuth sector at an incidence angle of 40° with an assumption of 0.2 dB instrumental noise at wind speeds of 2–30 m/s.

For that purpose, we performed simulations of the wind retrieval errors in the case of the semicircular scheme at an increased number of integrated NRCS samples in the azimuth sector. The simulations showed that to achieve error values in the semicircular scheme similar to errors in the whole 360° circular scheme, the number of integrated NRCS samples in the azimuth sector must be increased to about 261 (which is of course acceptable in practice, as the number of integrated samples was up to 5000 in the scatterometer observations reported by Nghiem et al., previously [34]). Figures 4 and 5 represent the simulation results of the wind retrieval errors in the case of the semicircular scheme when 261 NRCS samples are integrated in the azimuth sector, assuming a 0.2 dB instrumental noise at incidence angles of 30° and 40°, respectively. The wind retrieval maximum errors are 0.73 m/s and 5.2° at θ = 30°, and 0.68 m/s and 5.0° at θ = 40°.

Thus, our simulations proved that the semicircular scheme is well-suited to wind speed and direction retrieval, and the wind retrieval errors are within the typical errors of the scatterometer wind recovery of ±2 m/s and ±20° [35]. Although the semicircular scheme requires a number of integrated NRCS samples in the azimuth sector approximately three times higher than for the whole 360° circular scheme, it allows a maximum altitude of the wind retrieval method's applicability about double that of the whole 360° circular scheme.

Referring back to the HIWRAP system, application of the semicircular scheme could increase its wind retrieval applicability using our method up to 34.64 km and 23.84 km at the incidence angles of 30° and 40°, respectively. Thus, HIWRAP or a similar airborne conical scanning radar using the semicircular scheme of azimuth NRCS sampling, and the wind retrieval algorithm presented above could allow wind retrieval over the sea when the radar is mounted on a high-altitude UAV or aircraft with a ceiling of about 35.64 km, yet still providing the accuracy typical of wind measurement by a scatterometer.

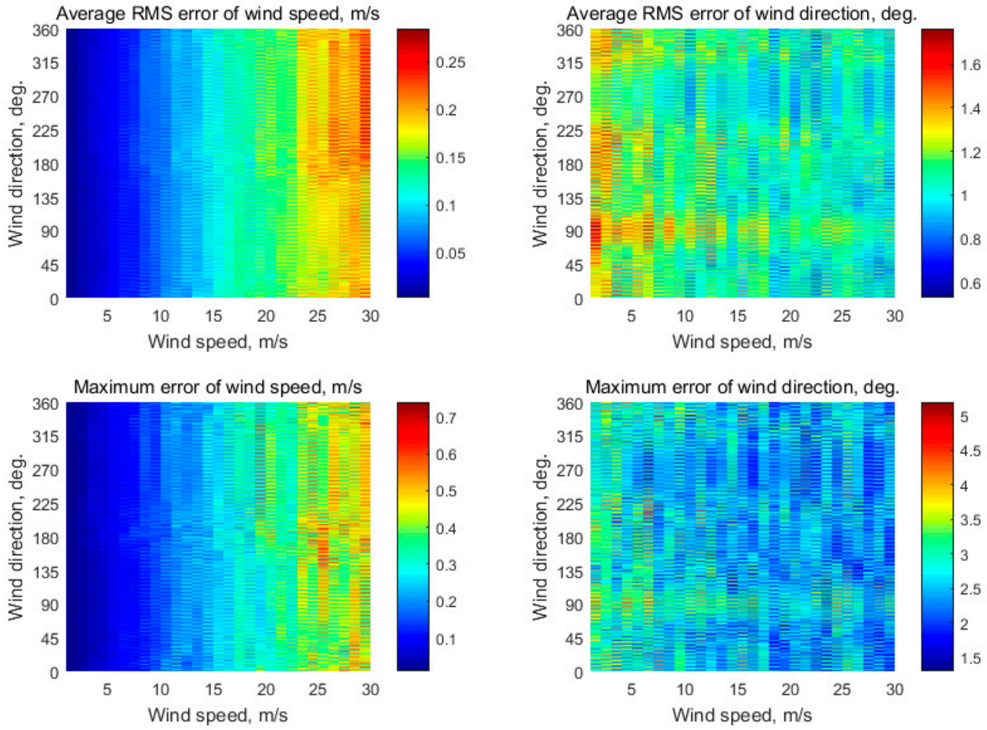

Figure 4. Simulation results in the case of the semicircular scheme (observation of N = 37 azimuth sectors at the directions of 0°, 5°, 10°, ... 180° relative to the aircraft's course) when 261 NRCS samples are integrated in each azimuth sector at an incidence angle of 30° with an assumption of 0.2 dB instrumental noise at wind speeds of 2–30 m/s.

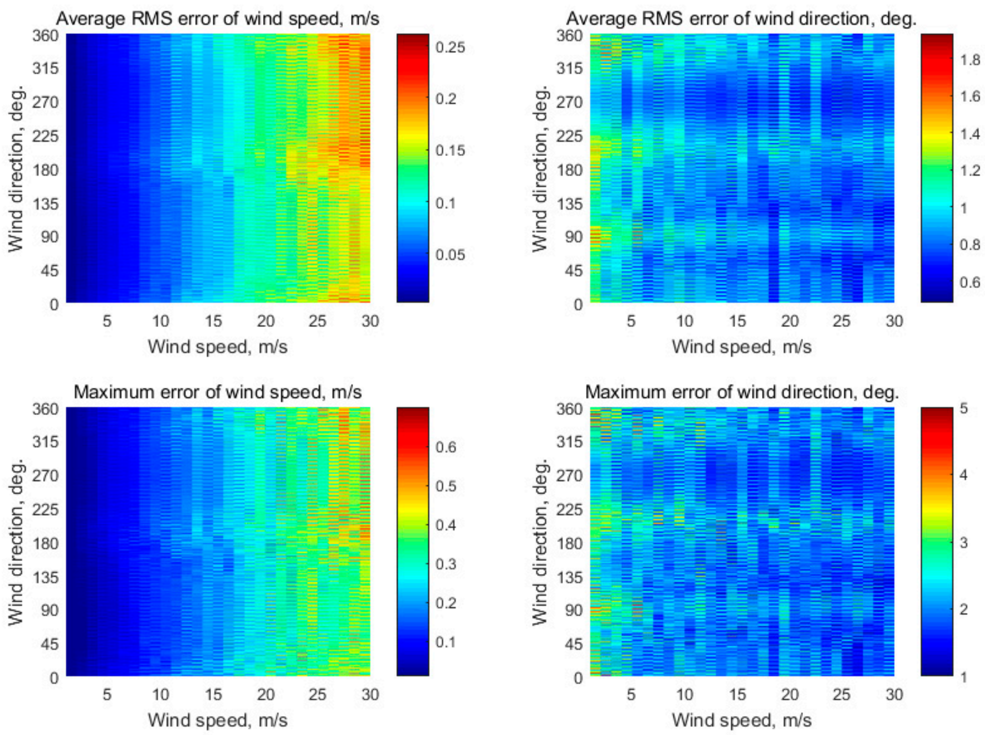

Figure 5. Simulation results in the case of the semicircular scheme (observation of N = 37 azimuth sectors at the directions of 0°, 5°, 10°, ... 180° relative to the aircraft's course) when 261 NRCS samples are integrated in each azimuth sector at an incidence angle of 40° with an assumption of 0.2 dB instrumental noise at wind speeds of 2–30 m/s.

Depending on the current altitude of the UAV or aircraft, the appropriate wind retrieval scheme and algorithm should be applied. For example, at an incidence angle of 30°, the whole 360° circular scheme with the appropriate number of NRCS samples integrated in each azimuth sector can be used up to about 17.32 km altitude, whereas the semicircular scheme with a correspondingly increased number of NRCS samples integrated in each azimuth sector can be used up to about 34.64 km altitude.

4. Conclusions

We investigated the possibility of increasing the maximum altitude of a wind retrieval method's applicability by using only half of the circular NRCS curve for wind measurement by a scatterometer mounted on a high-altitude remote sensing UAV or aircraft.

Our analysis of a conical scanning radar operated as a scatterometer mounted on a high-altitude UAV has shown that it is feasible for measuring sea-winds not only via the whole 360° circular scheme of azimuth NRCS sampling, but also by using a semicircular scheme of azimuth NRCS sampling. Splitting the whole 360° circular NRCS observation scheme in half allows separating the ground strip into two semicircular ground strips. Each semicircular strip is half the width of the equivalent circular ground strip, and so the semicircular scheme allows the maximum altitude of the method's applicability to be twice that of the circular scheme.

Simulations based on our new wind retrieval algorithm showed that a conical scanning radar operated in scatterometer mode using the semicircular scheme of azimuth NRCS sampling is entirely feasible for sea-wind measurements. However, to provide wind retrieval accuracy in the semicircular scheme similar to that of wind measurements using the whole 360° circular scheme, the semicircular scheme requires approximately three times higher the number of integrated NRCS samples in each azimuth sector than the circular scheme. Nonetheless, the accuracy of wind speed and direction retrieval using our new algorithms is within the range of typical scatterometer accuracy, i.e., ± 2 m/s and $\pm 20°$.

The semicircular scheme and associated wind retrieval algorithm increases HIWRAP's wind retrieval applicability up to 34.64 km at incidence angles of 30° and up to 23.84 km at incidence angles of 40°. Thus, the semicircular scheme and algorithm are applicable for airborne conical scanning radars mounted on high-altitude UAVs or aircraft with a ceiling of up to about 35.64 km.

To perform the wind measurements, the high-altitude UAV or aircraft should perform a horizontal straight flight. The antenna of the conical scanning scatterometer or multifunctional radars with the scatterometer mode should be stabilized in the horizontal plane.

The results obtained can be used for the enhancement of existing UAV and aircraft radars, and for the development of new remote sensing systems, extending their applications for standalone and joint measurements in oceanography, meteorology, and navigation.

Author Contributions: Conceptualization, A.N.; methodology, A.N., A.K., and C.F.; software, A.K.; validation, A.N., A.K., and C.F.; formal analysis, A.N. and A.K.; investigation, A.N., A.K., and C.F.; resources, A.K.; data curation, A.N. and A.K.; writing—original draft preparation, A.N.; writing—review and editing, A.N., A.K., and C.F.; visualization, A.N. and A.K.; supervision, A.N.; project administration, A.K.; funding acquisition, A.K. All authors have read and agreed to the published version of the manuscript.

Funding: This research was funded by the Russian Science Foundation grant number 21-79-10375, https://rscf.ru/en/project/21-79-10375/ (accessed on 22 August 2022). The APC was funded by the Russian Science Foundation grant number 21-79-10375.

Institutional Review Board Statement: Not applicable.

Informed Consent Statement: Not applicable.

Data Availability Statement: Data sharing not applicable.

Conflicts of Interest: The authors declare no conflict of interest.

References

1. Wikipedia. Unmanned Aerial Vehicle. Available online: https://en.wikipedia.org/wiki/Unmanned_aerial_vehicle (accessed on 22 August 2022).
2. International Trade Administration. Unmanned Aircraft Systems. Available online: https://www.trade.gov/unmanned-aircraft-systems (accessed on 22 August 2022).
3. Valavanis, K.P.; George, J.; Vachtsevanos, G.J. *Handbook of Unmanned Aerial Vehicles*; Springer: Dordrecht, The Netherlands, 2015; p. 3022. [CrossRef]
4. Njoku, E.G. *Encyclopedia of Remote Sensing*; Springer: New York, NY, USA, 2014; p. 939. ISBN 978-0-387-36700-2.
5. Nex, F.; Armenakis, C.; Cramer, M.; Cucci, D.A.; Gerke, M.; Honkavaara, E.; Kukko, A.; Persello, C.; Skaloud, J. UAV in the advent of the twenties: Where we stand and what is next. *ISPRS J. Photogramm. Remote Sens.* **2022**, *184*, 215–242. [CrossRef]
6. Wikipedia. List of Unmanned Aerial Vehicle Applications. Available online: https://en.wikipedia.org/wiki/List_of_unmanned_aerial_vehicle_applications (accessed on 22 August 2022).
7. Mohsan, S.A.H.; Khan, M.A.; Noor, F.; Ullah, I.; Alsharif, M.H. Towards the unmanned aerial vehicles (UAVs): A comprehensive review. *Drones* **2022**, *6*, 147. [CrossRef]
8. Guan, S.; Zhu, Z.; Wang, G. A review on UAV-based remote sensing technologies for construction and civil applications. *Drones* **2022**, *6*, 117. [CrossRef]
9. Basan, E.; Basan, A.; Nekrasov, A.; Fidge, C.; Sushkin, N.; Peskova, O. GPS-spoofing attack detection technology for UAVs based on Kullback–Leibler divergence. *Drones* **2022**, *6*, 8. [CrossRef]
10. Kurdel, P.; Češkovič, M.; Gecejová, N.; Adamčík, F.; Gamcová, M. Local control of unmanned air vehicles in the mountain area. *Drones* **2022**, *6*, 54. [CrossRef]
11. Yao, H.; Qin, R.; Chen, X. Unmanned aerial vehicle for remote sensing applications—A review. *Remote Sens.* **2019**, *11*, 1443. [CrossRef]
12. Pennsylvania State University. Classification of the Unmanned Aerial Systems. Available online: https://www.e-education.psu.edu/geog892/node/5 (accessed on 22 August 2022).
13. Singhal, G.; Bansod, B.; Mathew, L. Unmanned aerial vehicle classification, applications and challenges: A review. *Preprints* **2018**, 2018110601. [CrossRef]
14. Bard College Center for the Study of the Drone. High-Altitude Drones. Available online: https://dronecenter.bard.edu/high-altitude-drones (accessed on 22 August 2022).
15. Li, L.; Heymsfield, G.; Carswell, J.; Schaubert, D.H.; McLinden, M.L.; Creticos, J.; Perrine, M.; Coon, M.; Cervantes, J.I.; Vega, M.; et al. The NASA high-altitude imaging wind and rain airborne profiler. *IEEE Trans. Geosci. Remote Sens.* **2016**, *54*, 298–310.
16. NASA Goddard Space Flight Center. HIWRAP. Available online: https://har.gsfc.nasa.gov/index.php?section=13 (accessed on 22 August 2022).
17. Guimond, S.R.; Tian, L.; Heymsfield, G.M.; Frasier, S.J. Wind retrieval algorithms for the IWRAP and HIWRAP airborne Doppler radars with applications to hurricanes. *J. Atmos. Ocean. Technol.* **2014**, *31*, 1189–1215. [CrossRef]
18. Nekrasov, A.; De Wit, J.J.M.; Hoogeboom, P. FM-CW millimeter wave demonstrator system as a sensor of the sea surface wind vector. *IEICE Electron.* **2004**, *1*, 137–143. [CrossRef]
19. Nekrasov, A. *Airborne Doppler Navigation System Application for Measurement of the Water Surface Backscattering Signature, Proceedings of the ISPRS TC VII Symposium—100 Years ISPRS, Vienna, Austria, 5–7 July 2010*; Wagner, W., Székely, B., Eds.; The International Archives of the Photogrammetry, Remote Sensing and Spatial Information Sciences: Hannover, Germany, 2010; pp. 163–168, XXXVIII, Part 7A; Available online: https://www.isprs.org/proceedings/XXXVIII/part7/a/pdf/163_XXXVIII-part7A.pdf (accessed on 22 August 2022).
20. Nekrasov, A. Measuring the sea surface wind vector by the Doppler navigation system of flying apparatus having the track-stabilized four-beam antenna. In Proceedings of the 17th Asia Pacific Microwave Conference (APMC), Suzhou, China, 4–7 December 2005; Volume 1, pp. 645–647. [CrossRef]
21. Nekrasov, A.; Dell'Acqua, F. Airborne Weather Radar: A theoretical approach for water-surface backscattering and wind measurements. *IEEE Geosci. Remote Sens. Mag.* **2016**, *4*, 38–50. [CrossRef]
22. Nekrasov, A.; Veremyev, V. Airborne weather radar concept for measuring water surface backscattering signature and sea wind at circular flight. *Nase More* **2016**, *63*, 278–282. [CrossRef]
23. Nekrasov, A.; Khachaturian, A.; Abramov, E.; Popov, D.; Markelov, O.; Obukhovets, V.; Veremyev, V.; Bogachev, M. Optimization of airborne antenna geometry for ocean surface scatterometric measurements. *Remote Sens.* **2018**, *10*, 1501. [CrossRef]
24. Nekrasov, A.; Khachaturian, A. Towards the sea wind measurement with the airborne scatterometer having the rotating-beam antenna mounted over fuselage. *Remote Sens.* **2021**, *13*, 5165. [CrossRef]
25. Nekrasov, A.; Khachaturian, A.; Vorobev, E. Optimization of the NRCS sampling at the sea wind retrieval by the airborne rotating-beam scatterometer mounted under fuselage. *Sensors* **2022**, *22*, 4016. [CrossRef] [PubMed]
26. Nekrassov, A. Sea surface wind vector measurement by airborne scatterometer having wide-beam antenna in horizontal plane. In Proceedings of the IGARSS'99, Hamburg, Germany, 28 June–2 July 1999; Volume 2, pp. 1001–1003. [CrossRef]
27. Nekrassov, A. On airborne measurement of the sea surface wind vector by a scatterometer (altimeter) with a nadir-looking wide-beam antenna. *IEEE Trans. Geosci. Remote Sens.* **2002**, *40*, 2111–2116. [CrossRef]

28. Nekrasov, A.; Khachaturian, A.; Veremyev, V.; Bogachev, M. Doppler navigation system with a non-stabilized antenna as a sea-surface wind sensor. *Sensors* **2017**, *17*, 1340. [CrossRef]
29. Spencer, M.W.; Graf, J.E. The NASA scatterometer (NSCAT) mission. *Backscatter* **1997**, *8*, 18–24.
30. Hans, P. *Auslegung und Analyse von Satellitengetragenen Mikrowellensensorsystemen zur Windfeldmessung (Scatterometer) Über Dem Meer und Vergleich der Meßverfahren in Zeit- und Frequenzebene. Von der Fakultät 2 Bauingenieur- und Vermessungswesen der Universität Stuttgart zur Erlangung der Würde eines Doktor-Ingenieurs Genehmigte Abhandlung*; Institut für Navigation der Universität Stuttgart: Stuttgart, Germany, 1987; Volume 225 S. (In German)
31. Ulaby, F.T.; Long, D.G. *Microwave Radar and Radiometric Remote Sensing*; University of Michigan Press: Ann Arbor, MI, USA, 2014; p. 1116. ISBN 978-0-472-11935-6.
32. Nekrasov, A.; Khachaturian, A.; Abramov, E.; Markelov, O.; Bogachev, M. On Sea Ice Measurement by a C-Band Scatterometer at VV Polarization: Methodology Optimization Based on Computer Simulations. *Remote Sens.* **2019**, *11*, 2518. [CrossRef]
33. Lin, W.; Portabella, M.; Stoffelen, A.; Verhoef, A. On the characteristics of ASCAT wind direction ambiguities. *Atmos. Meas. Tech.* **2013**, *6*, 1053–1060. [CrossRef]
34. Nghiem, S.V.; Li, F.K.; Lou, S.-H.; Neumann, G.; McIntosh, R.E.; Carson, S.C.; Carswell, J.R.; Walsh, E.J.; Donelan, M.A.; Drennan, W.M. Observations of radar backscatter at Ku and C bands in the presence of large waves during the Surface Wave Dynamics Experiment. *IEEE Trans. Geosci. Remote Sens.* **1995**, *33*, 708–721. [CrossRef]
35. Komen, G.J.; Cavaleri, L.; Donelan, M.; Hasselmann, K.; Hasselmann, S.; Janssen, P.A.E.M. *Dynamics and Modelling of Ocean Waves*; Cambridge University Press: Cambridge, UK, 1994; p. 532.